PRAMANA
— journal of
physics

© Printed in India

Vol. 46, No. 5,
May 1996
pp. 357–372

Effective potentials and threshold anomaly

S V S SASTRY and S K KATARIA
Nuclear Physics Division, Bhabha Atomic Research Centre, Bombay 400 085, India

MS received 22 September 1995; revised 16 January 1996

Abstract. The strong E and L dependence of the effective elastic channel potentials is shown to be an implicit radial kinetic energy (ε) dependence. It is also shown that this effective potential satisfies the dispersion relation in ε variable at the strong absorption radius. Further, the experimental data for both elastic and fusion channels are consistent with this L-dependence of the corresponding effective potentials. The effective transfer channel potentials derived using CRC code FRESCO are shown to exhibit strong energy dependence as a result of couplings. The energy dependence of effective transfer strength for $^{16}O + ^{208}Pb$ and $^{16}O + ^{232}Th$ systems is determined using the experimental transfer angular distributions.

Keywords. Effective potentials; TELP; threshold anomaly; dispersion relation; CRC calculations; fusion.

PACS No. 24·10

1. Introduction

The optical model (OM) study of elastic scattering of heavy ions near the Coulomb barrier energies has resulted in many interesting observations. At energies well above the Coulomb barrier, it is well known that the scattering process is much simpler as in the case of point particles and the corresponding optical model potentials (OMP) are static or vary weakly with energy. In depth OM studies around the Coulomb barrier energies and below, have shown that the OMP parameters strongly vary with energy. This phenomenon is known as threshold anomaly (TA) [1]. In optical model analysis, where the potential strength parameters alone are varied, it was shown that the real part of the nuclear potential becomes more attractive around the barrier energies and decreases on either side, thus resulting in a bell-shaped curve. The imaginary part which remains more or less constant at high energies, decreases sharply with decreasing energy below the Coulomb barrier as observed in OM analysis of several heavy ion systems like $^{16}O + ^{60}Ni$, $^{16}O + ^{208}Pb$, $^{32}S + ^{64}Ni$, $^{32}S + ^{40}Ca$, $^{16}O + ^{63}Cu$, [2, 3] and $^{16}O + ^{209}Bi$ [4]. The reader may refer to the detailed review by Satchler [3] and the references therein. In a nonrelativistic formalism, it is known that the causality condition on potential and the quantum mechanical wave function results in Cauchy's integral relation between the real (V) and imaginary (W) parts of the OMP [1, 3], as stated by

$$V(E) = \frac{1}{\pi} P \int_{-\infty}^{\infty} \frac{W(E')}{(E - E')} \mathrm{d}E', \tag{1}$$

where P stands for the principle part of the integral. Equation (1) is also known as dispersion relation (DR). Therefore, the energy dependence of imaginary part implies energy dependence in real part and vice versa. This contribution to the OMP is also called dynamic polarization potential. By normalizing the strength of the real potential at a high energy point E_s, (1) can be generalized as [5],

$$V(r, E) = V(r, E_s) + \Delta V(r, E) \tag{2}$$

with,

$$\Delta V(r, E) = \frac{(E - E_s)}{\pi} P \int_{-\infty}^{\infty} \frac{W(r, E')}{(E - E')(E_s - E')} dE'. \tag{3}$$

Equation (3) suggests that the energy dependence of real and imaginary parts of OMP is related but does not rule out any other energy dependence besides that coming through eq. (2). For example, the effective momentum and energy dependence can arise from non-local part of the interaction or intrinsic energy dependence and it is not obvious that such a potential will obey a dispersion relation (DR). However if eq. (3) is satisfied, then the effective nuclear potential becomes more attractive at around the barrier energies and results in energy dependence of the barrier height. This energy dependence of OMP is only qualitatively in conformity with the conclusions drawn from the studies of fusion channel. In fusion studies, the experimental data can be summarized as (i) the cross section enhancement at sub-barrier energies and (ii) the broadening of the spin distribution around and below the barrier energies. It was proposed that these results can be accounted for in the barrier penetration model (BPM) if the fusion barrier height is made energy-dependent. However, the energy dependent part, derived from the elastic channel scattering data does not reproduce the fusion cross section enhancement quantitatively [2, 5]. Further, the energy dependence of the effective barrier height even when adjusted to account for the fusion cross-section, fails to account for the fusion spin distribution. Therefore, the effective barrier height and hence the effective heavy ion potential is known to be both E and L dependent in order to be consistent with experimental fusion spin distribution. It was shown earlier [6] that the fusion data can be well described in the BPM if the fusion barrier height depends implicitly on E and L through a variable ε, the radial kinetic energy at the interaction barrier. Similar conclusions were also drawn for the OM effective fusion potential [7–9]. Therefore, it is expected that the effective heavy ion potential for the elastic channel also be L dependent and this dependence must be consistent with DR for effective potentials. In contrast to this, the OM analysis of elastic angular distributions does not demand a serious need for this L dependence, even though strong energy dependence is found to be necessary. Hence there is an anomaly between the elastic and fusion channel potentials with respect to L dependence. In order to understand this anomaly one needs to study this L dependence of effective elastic channel potential used in OM analysis. It should be noticed that OM analysis of elastic scattering data is not a very sensitive test for the L dependence since the angular distributions around the barrier energies are featureless and do not vary strongly with angle. Therefore, we have studied the L-dependence of effective potentials based on the coupled reaction channel (CRC) results obtained using the code FRESCO.

The CRC formalism has been very successful in describing the heavy ion reaction mechanism [2]. In this formalism, all the important reaction channels are coupled together and the CRC solution is obtained by iteration. Fusion is estimated as the flux removed from the coupled channels system by the use of OM imaginary potential (W) in each channel or by means of ingoing wave boundary condition. We have studied the $^{16}O + ^{208}Pb$ system with the coupling scheme as well as the coupling parameters taken from [2]. The energy dependence of effective potential and their dispersive nature are also discussed in detail in [2]. These calculations show that the fusion and reaction excitation functions are well described, in addition to inelastic and transfer cross sections. The method gives reasonably good predictions for elastic angular distributions and the observed TA of effective potentials. However, there are still some important shortcomings as discussed below:

(i) the fusion mean square spin does not agree with the experimental data at low energies.
(ii) the elastic angular distributions predicted are not in very good agreement with the experimental data for near barrier energies and in addition there is a backward angle enhancement of elastic cross section compared to experimental data [2, 10].
(iii) the polarization potentials derived are not in good agreement with dispersion relation over a wide energy range [2].
(iv) the derived energy dependent effective barrier, when used in the standard barrier penetration model, does not reproduce the CRC fusion excitation function at low energies [2].

In the present work, we study the energy dependence of effective potentials as a result of couplings for elastic, fusion and transfer channels. In the first section, the E and L dependence of the effective elastic channel potential obtained using CRC wave functions and the dispersion relation for these potentials are presented. Further, the E and L dependences of these potentials are shown to be consistent with the implicit dependence through a single variable ε to a good approximation. In the second section, the ε dependent potentials are shown to reproduce experimental results for both elastic and fusion channels. In the third section, the effective one channel transfer strength parameter derived from CRC results is shown to be energy dependent similar to effective elastic channel potentials. Use of this effective particle transfer strength in the CCFUS code yields better estimates for the fusion cross section and its mean square spin values.

2. Effective elastic channel potentials

The CRC calculations have been performed over a wide energy range and the elastic wave functions are obtained for each partial wave. In order to understand the TA, one needs to construct local polarization potentials using this CRC wave function. There are many ways of deriving the local polarization potentials [2, 10, 11]. In the first method, one obtains the local effective elastic channel potential from the condition that it must reproduce the CRC elastic wave function at every point (r) as given by

$$[T + V_{\text{eff}}(r) + V_C(r) + V_L(r)]\psi_{\text{el}}^{\text{CRC}}(r) = E\psi_{\text{el}}^{\text{CRC}}(r), \tag{4a}$$

where

$$V_{\text{eff}}(r) = V_N^{\text{bare}}(r) + V_{\text{pol}}(r). \tag{4b}$$

This is equivalent to the potential derived from the OM fits of elastic angular distributions as given in eq. (2),

$$V_{\text{eff}}(r) = V(r, E). \tag{4c}$$

Here, V_N is the bare nuclear part of heavy ion potential for elastic channel, as used in the CRC calculations. The second term V_{pol} includes all the effects of the channel couplings on the elastic channel wave function. The V_{eff} defined in this way is known as trivially equivalent local potential (TELP) which is wave function equivalent [2] and can be obtained numerically using (4a), provided the wavefunction at the point r, does not vanish. In the second approach, V_{pol} is obtained from the effective potentials that reproduce the S-matrix elements for each partial wave [10]. There are also attempts to obtain V_{pol} by inverting the fusion cross section data at each energy [11]. However, one should notice that such an inversion gives effective fusion barrier and hence the derived polarization contribution will not be in agreement with the elastic channel potential. This discrepancy between the effective elastic channel potential and the fusion barrier has been discussed earlier in the introduction. In addition, such a polarization potential may not be consistent with the fusion spin distributions.

The TELP strongly depend on E and L and especially the imaginary part can be emissive as well as absorptive as a function of r, destroying the flux conservation for each channel. This is because the flux from one channel at a point r and the partial wave L can be removed and added at a point r' at L' to the same or different channel. This rearrangement of flux takes place for a given energy and total angular momentum consistent with the flux conservation over all the channels in the CRC calculations. It is not obvious that such a nonlocal effect is reducible to an effective local and dispersive potentials and therefore, the DR is a stringent condition to be verified in these calculations. For the purpose of studying DR, there are attempts to obtain the weighted L-averaged polarization potential (which depends only on energy) using the TELP. However as discussed earlier, this energy dependent potential when incorporated in a BPM, could not reproduce even the CRC fusion cross sections at low energy [2]. Thus, any choice of L-averaging may not be good enough. In order to establish a DR, (3) should be applied to the imaginary part of TELP under the assumption that it is applicable to each partial wave (total J). The applicability of DR to weighted L-independent potential requires explicit justification since only one weighting procedure is likely to satisfy DR as the weight factors involve energy dependence. Here we present the results for TELP at a fixed radial separation.

Figure 1 shows the TELP as a function of L for five different bombarding energies [10] at $R_s = 12{\cdot}5$ fm, which is the strong absorption radius. The radial distribution of flux in the reaction channel peaks at this radius and therefore, the effective potential strength is important around this radial separation. As seen in figure 1, the real and imaginary parts of TELP show rapid variation as a function of L in addition to undulations which are difficult to eliminate. The L-weighted procedure can be seen to be averaging over many important features of the TELP and results in a mean potential which varies smoothly with energy. For example at 96 MeV, (see figure 1) the real part

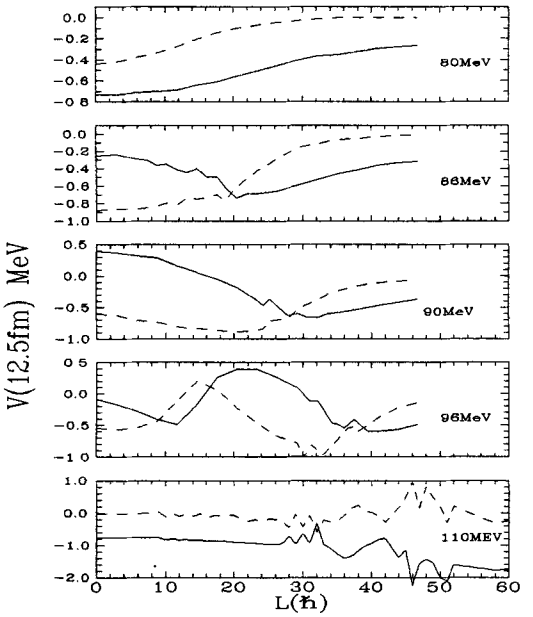

Figure 1. L versus real part of TELP (solid curve) and imaginary part of TELP (dashed curve), obtained from the CRC elastic wave function at $R_s = 12{\cdot}5$ for different incident energies as mentioned in the plots. This and all subsequent figures refer to the system $^{16}O + ^{208}Pb$.

becomes repulsive for L-values around $27\hbar$ to $30\hbar$ and becomes attractive beyond. The imaginary part also exhibits emissive and absorptive behaviour and is strongly absorptive for $L \approx 25\hbar - 30\hbar$. It is to be noticed that the hump seen in the L-distribution for 96 MeV is absent in the case of 90 MeV. At this energy the TELP is both increasing and decreasing as a function of L, whereas at 80 MeV the potentials vary monotonically with L. One interesting point to observe in figure 1 is that the large L behaviour of TELP at 96 MeV is similar to the low L behaviour at 90 MeV. Similar observation can be made for any two sets of neighbouring plots of figure 1 and the most prominent are the cases of 80 MeV and 86 MeV. These correlations suggest that the TELP may not depend explicitly on E and L but have implicit dependence through ε, similar to the case of effective fusion potentials.

Figure 2a shows the L-dependence of imaginary part of TELP for all the cases of figure 1, plotted as a function of ε. The E_{rot} is evaluated at $R_s = 12{\cdot}5$ fm. As seen in the figure, the widely different cases of figure 1 merge into a single curve on ε scale showing the validity of the proposed E and L dependence through ε. It also suggests that there is no need to construct L-independent potentials in order to study their dispersive nature. This is a total departure from the methods followed in earlier studies. This ε dependent effective elastic channel potential gives rise to ε dependent effective barrier and thus relates well with the ε dependence of the potentials derived from fusion studies [7]. This procedure eliminates the need of arbitrary weight factors. However, this ε dependence of effective potentials does not smooth out the observed strong oscillations in the

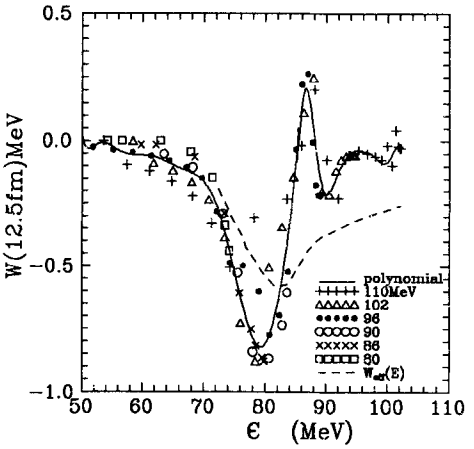

Figure 2a. Imaginary part of the TELP versus ε for different symbols as described in the figure. The continuous curve is a polynomial fit to the data. The dashed curve represents the weighted mean energy dependent potential.

L-dependence but rather transforms into a general behaviour at high energies. Generalizing the DR to each partial wave (of elastic channel), from (3) we get,

$$\Delta V(r,E,L)=\frac{(E-E_s)}{\pi}P\int_{-\infty}^{\infty}\frac{W(r,E',L)}{(E-E')(E_s-E')}\mathrm{d}E'. \tag{5}$$

As a consequence of ε dependence of W i.e., $W(E,L)=W(\varepsilon,0)$, eq. (5) can be transformed into ε scale. The strong absorption radius, R_s (which is used to define ε), depends weekly on energy and to a first approximation it can be neglected. From this it follows

$$\Delta V(r,\varepsilon)=\frac{(\varepsilon-\varepsilon_s)}{\pi}P\int_{-\infty}^{\infty}\frac{W(r,\varepsilon)}{(\varepsilon-\varepsilon')(\varepsilon_s-\varepsilon')}\mathrm{d}\varepsilon'. \tag{6}$$

It is to be noticed that E_s is a fixed quantity in eqs (3, 5) and similarly ε_s is also taken to be a fixed quantity in (6). Thus (6) is not simply a transformation of (5) but in a way ε replaces in it the dynamical role of E of (5). The LHS of (6) is the dispersion contribution to the real part induced by the energy dependence of imaginary part of TELP. Therefore the validity of DR for effective potentials can be verified by checking the equality of $\Delta V(r,\varepsilon)$ and the energy dependence of real polarization part of the TELP, i.e. V_{pol} of eq. (4).

Figure 2b shows the L-dependence of real part of TELP (represented by various symbols) for different cases of figure 1, plotted as a function of ε. The TELP for different energies and L values of figure 1 merge into a single curve on ε scale, similar to the case in figure 2a. The dispersion result obtained by applying (6) to the imaginary part of TELP is shown by solid curve. The agreement between these two cases (symbols and solid curve) implies that the ε dependence of real part of the TELP is accounted by DR to a good approximation and thus verifies the validity of DR on ε scale. The L-averaged energy dependent potentials are obtained from the TELP with reaction L-distributions

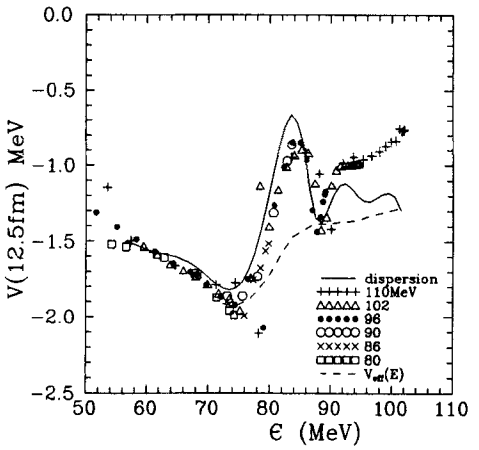

Figure 2b. Same as figure 2a, but for the real part of TELP. The solid curve is the dispersion contribution corresponding to the solid curve of figure 2a. The dashed curve is the weighted mean energy dependent potential.

as weight factors. This averaging gives rise to smooth energy dependence and is also shown in figures 2(a, b) as dashed curves. The imaginary part of TELP as a function of ε is small at high energies. Therefore at this radial separation, the absorption of flux into reaction channel is smaller for low partial waves as compared to larger partial waves. The large backward angle enhancement predicted by CRC calculations for elastic channel may be understood in terms of this weak imaginary potential for low partial waves at high energy. The oscillations in $W(\varepsilon)$ at high energy are due to the strong oscillations in the asymptotic wave function with energy at a given radial separation ($R_s = 12{\cdot}5$ fm). The imaginary potential shows maximum absorption around the barrier energies and the corresponding real part shows maximum attraction at these ε values (figure 2b).

Thus, it is shown that the energy dependence of real and imaginary parts of TELP are consistent with DR at strong absorption radius. However, (6) implies that the DR is also valid at other radial separations. In order to study this, the TELP were obtained at 10 and 11 fm for 110 and 102 MeV bombarding energies.

Figure 2c shows the real (bare potential subtracted) and imaginary parts of TELP at these radial separations represented by symbols. The E_{rot} is evaluated at the corresponding radii. The solid curves shown in the real potentials are obtained by applying (6) to the solid curves in imaginary parts (polynomial fits). The agreement of symbols and the solid curves in the real potentials shows the approximate validity of the DR at these radial separations. To these dispersion corrections at a given radius, one must add a static potential to match with the real part of TELP (see (2) and (4c)). The static potentials required at 10, 11 and 12·5 fm are respectively $-35{\cdot}1$, $-5{\cdot}2$ and $-1{\cdot}25$ MeV and the total potential compares well with the phenomenological potentials of Kim *et al* [7]. The imaginary part of TELP in figure 2c shows rapid variation around 90 MeV and in this energy region, the real part also shows strong energy dependence. It can be seen from figure 2c that the imaginary potential at 90 MeV is absorptive for 11 fm whereas it is emmissive for 10 fm.

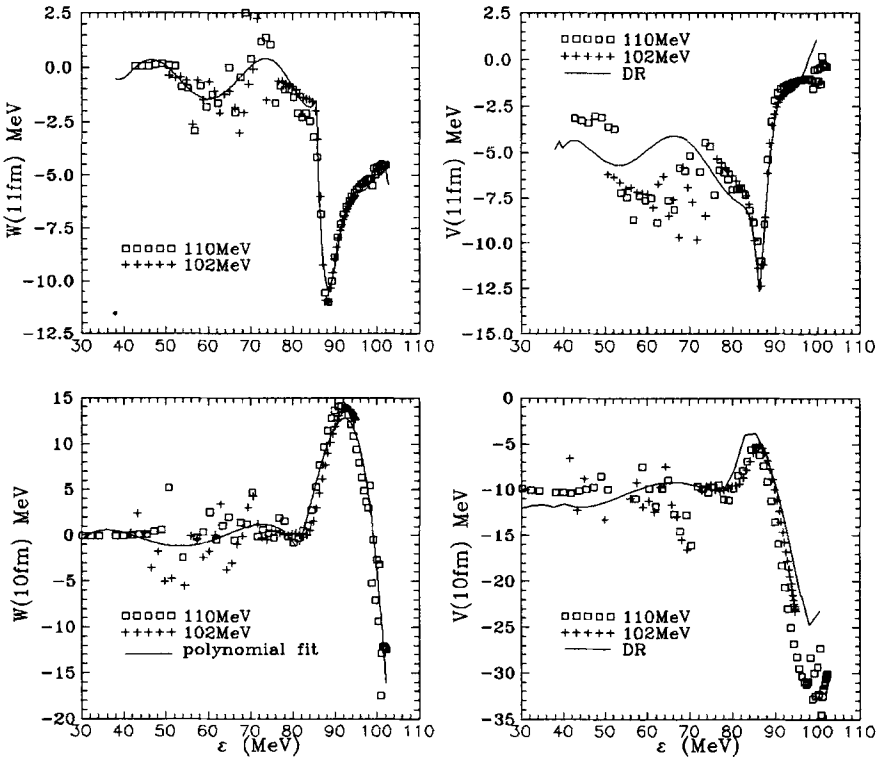

Figure 2c. Imaginary and real parts of TELP versus ε at the radial separations of 10 and 11 fm. The symbols used are explained in the figure. The solid curves in the imaginary potentials are the polynomial fits. The solid curves in the real potentials are obtained by applying the dispersion integral to solid curves of the imaginary potentials.

At large distances it is difficult to obtain the TELP from CRC wave functions reliably using present method. At large radii, the wave function is large in magnitude, the expected polarization potential is small and numerical accuracies pose a problem. Therefore, this study has not been extended for radii beyond 13 fm. At small distances the wave function decreases in magnitude and obtaining effective potentials which are of large strength also is difficult. Further, for the radial separations for which the validity of DR has been presented, the dispersion integral is applied in a limited energy region where the imaginary part of TELP is obtained from CRC calculations. In both cases (of small and large distances), one needs a coupled channel wave function at a very small step size to determine the kinetic energy accurately in order to obtain correct effective potentials. This requires enormous computation time and memory.

The TELP are explicitly dependent on radial separation, energy and angular momentum. This method of analysis of studying the DR at fixed radial separation assumes that the imaginary potential can be factorized into radial and energy dependence (for example, see (7b)). This is commonly used and is a good approximation for energies around the barrier region, where the polarization effects are known to be maximum. However, the disagreement of dispersion correction with the real part of

TELP shown in figure 2b (see beyond 96 MeV) may be suggesting that this factorization may not be valid at high energies and large radial separations. The use of ε scale to study the dispersion relation instead of explicit E and L dependence is for its simplicity and it may be a good approximation only around the Coulomb barrier. At high energies, inversion gives potentials that do not converge.

3. Dynamical potentials for fusion

In the previous section, it was shown that effective elastic channel potentials obtained from CRC calculations are dependent on a variable ε and that the derived real and imaginary parts obey DR. However, as stated in the introduction, the strong L dependence was not realised in the OM analysis of experimental elastic data. Therefore it is necessary to show that experimental elastic angular distributions as well as the fusion data are consistent with the ε dependent effective potentials using the optical model analysis. The optical model code SNOOPY was modified to incorporate the proposed ε dependence (defined at the strong absorption radius) as given in (6) to the real and imaginary parts of OMP. Following [7], the ε dependence of W is factorized into inverse Woods–Saxon form and the r dependence of OMP is a Woods–Saxon type, as given by

$$V(r,\varepsilon) = \frac{V_0}{1+e^{(r-r_0)/a_0}} + V_p(r,\varepsilon), \tag{7a}$$

$$W(r,\varepsilon) = f(r)g(\varepsilon) \tag{7b}$$

with,

$$f(r) = \frac{W_0}{1+e^{(r-r_i)/a_i}}, \tag{7c}$$

$$g(\varepsilon) = \frac{1}{1+e^{(\varepsilon_0-\varepsilon)/a_\varepsilon}}. \tag{7d}$$

Here, $V_p(r,\varepsilon)$ is obtained by using (6) and $W(r,\varepsilon)$. It is not obvious that a strong L-dependent potential (through ε variable) can give good fits to elastic angular distributions. Figure 3 shows the OM fits to elastic data by this method represented by circles, from very high energy of 129·5 MeV to a low energy of 78 MeV (up to 80 MeV in the figure). The best OM fits to experimental data as reported in [12, 13, 14] are shown by solid curves. In trying to obtain good fits, R_s was varied with energy. The variation of R_s for different bombarding energies is given in table 1. This dependence compares well with the findings of Videbaek *et al* [12] only at low energies. However at high energies, the reaction is dominated by fusion which takes place around the barrier radius (fusion radius), and therefore, the strong absorption radius is also expected to approach fusion radius.

The reaction cross-section obtained from the present method is given in table 1 along with the results of simple energy dependence of OMP as reported by Kim *et al* [5]. The CRC results [2] and the experimental data [12, 13, 14] are also shown. As shown in the table, the reaction excitation function from the present analysis compares well with the results of various methods. This is expected as the angular distributions compare well with the distributions obtained from the corresponding methods (figure 3).

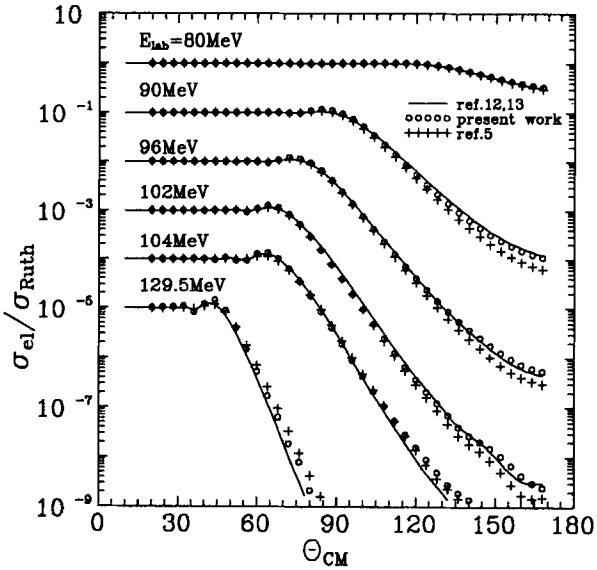

Figure 3. Elastic to Rutherford ratio as a function of θ_{cm} for different energies for the $^{16}O + ^{208}Pb$ system. The solid curves represent the best OM fits to experimental data as reported in refs [12, 13, 14]. The plus symbols represent the results of [5]. The circles represent the fits by present method and the OMP parameters used are as follows: $V_0 = 100$ MeV, $W_0 = 70$ MeV, $r_0 = r_i = r_c = 1{\cdot}23$ fm, $a_0 = a_i = 0{\cdot}49$ fm, $\varepsilon_s = 102$ MeV, $\varepsilon_0 = 78$ MeV and $a_\varepsilon = 4$ MeV. The plots at different energies are successively scaled down by a decade.

Table 1. Reaction excitation function by various methods.

E_{lab} MeV	R_s fm	σ_R(A) mb	σ_R(B) mb	σ_R(C) mb	σ_R(expt.) mb
78	12·5	37·5	49·4	41	45·7
80	12·5	99	123	101	100 ± 10
82	12·5	195			
83	12·5	248	290	259	237 ± 20
84	12·5	301			
86	12·5	406	461	425	440
88	12·5	507	568	529	570 ± 58
90	12·5	603	669	629	578 ± 55
96	12·5	867	940	899	904
102	12·5	1099	1173	1134	1147 ± 95
104	11·0	1117	1244		
110	11·0	1300	1440		
129·5	10·5	1724	1943		

A = present method using ε dependent potentials; B = method of Kim *et al* [5] using energy dependent potentials; C = CRC method using FRESCO; expt. = Experimental data [12, 13, 14].

Table 2. Excitation function and the $\langle L^2 \rangle$ for fusion by various methods.

E_{lab} MeV	σ_f A	$\langle L^2 \rangle$ A	σ_f B	$\langle L^2 \rangle$ B	σ_f C	$\langle L^2 \rangle$ C	σ_f expt.	$\langle L^2 \rangle$ expt.
78	10·96	173	9·0	109	6	104	$5{\cdot}6 \pm 0{\cdot}6$	170 ± 30
80	34·3	186	39	138	37	107	36 ± 4	200 ± 20
82	77·3	229						
83	105	259	127	224	157	195	108 ± 10	270 ± 40
84	135	291						
86	205	361	225	336	297	314	235	
88	283	435	290	415	385	400	350 ± 40	
90	367	512	352	496	466	488	377 ± 50	430
96	634	765	534	746	683	754	685 ± 70	
102	888	1044	725	1004	884	1000	844 ± 90	
104	825	999						
110	1009	1248	920	1346			1060 ± 50	1275
129·5	1376	1945	1353	2234			1315 ± 65	2085

A, B, C and expt. are as in table 1; σ_f = fusion cross section in mb; $\langle L^2 \rangle = L(L+1)$ in units of $\hbar^2$.

In direct reaction theory, the fusion cross-section is estimated as the overlap integral of the elastic wave function with the fusion potential [5, 7]. The radial and energy dependence of the fusion potential was factorized as $W_F(r, \varepsilon) = f(r) g_F(\varepsilon)$. The radial dependence $f(r)$ is taken to be same as that of reaction potential (eq. (7c)). The parameters of $g_F(\varepsilon)$ are determined by fitting the fusion excitation function by varying only one parameter (ε_0). The optimum value ε_0 of g_F is 84 MeV and a_e is same as that of reaction potential. As listed in table 2, the fusion excitation function is well reproduced showing the quality of the fit with one parameter. The resulting fusion mean square spin is also listed in the table. It can be seen that the fusion mean square spin agrees well with the experimental data at all energies, especially at low energies. At low energy of 78 MeV, the present method gives higher fusion cross section compared to experimental data. However when the parameters of g_F are adjusted to reproduce the data at this energy, the fusion $\langle L^2 \rangle$ still remains the same. The experimental data, CRC fusion results [2] and the results of Kim *et al* [5] are also listed in table for comparison. In other words, the L dependent potentials are in agreement with the experimental data for both elastic and fusion channels.

4. Dynamical potentials for transfer channel

The elastic and fusion channel effective potentials have been shown to be energy dependent as a result of couplings. Similarly, the effective potentials that describe transfer angular distributions for different transfer channels in a heavy ion collision are also expected to be energy dependent. The imaginary ptoential for direct reactions consisting of inelastic and transfer channels can be obtained as the difference of potentials for total reaction and fusion (§ 3) and this will also depend on ε. However, it is difficult to decompose this part into the components responsible for individual inelastic and transfer channels. In addition, such a partition of imaginary reaction potential into

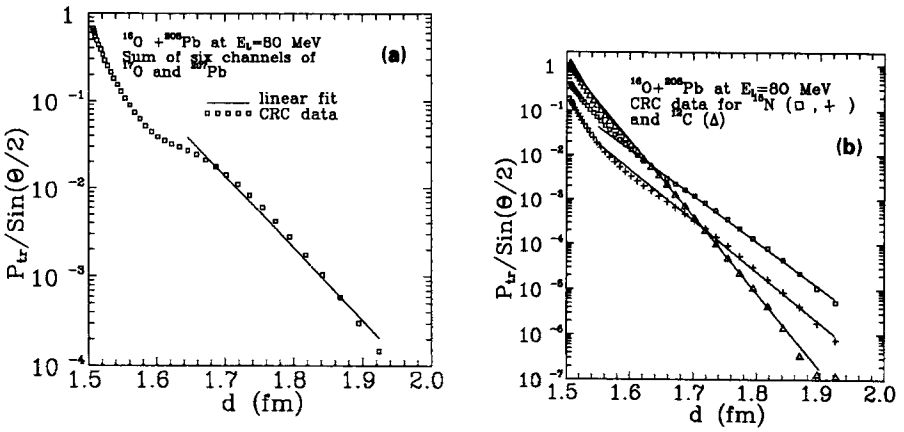

Figure 4. $P_{tr}/\sin(\theta/2)$ versus semi-classical distance of closest approach parameter, d, for neutron transfer (**a**), proton and alpha transfer channels (**b**) obtained from CRC transfer results at 80 MeV. For details see text.

its constituent channels only gives the respective partial wave distributions for various channels, whereas for the transfer angular distributions one needs phase information. Therefore, we adopt a semiclassical approach to estimate the effective one channel particle transfer strength function. In this formalism, the transfer angular distribution as a function of semi-classical distance of closest approach [15] is given by

$$P_{tr}(\theta, Q) = \frac{N}{\alpha^3} \sin\frac{\theta}{2} e^{-2\alpha(D-D_c)} e^{-(Q-Q_{opt})^2/2\sigma^2}, \tag{8a}$$

with

$$D = \frac{Z_p Z_t e^2}{2E_{cm}} \left(1 + \mathrm{cosec}\frac{\theta}{2}\right) = d(a_t^{1/3} + a_p^{1/3}), \tag{8b}$$

and the transfer form factor (strength function) is given by

$$F(r) = \frac{f_0}{r} e^{-\alpha(r-D_c)}. \tag{8c}$$

From these relations, $P_{tr}(\theta)$ can be obtained by integrating over the Q variable, with Q_{opt} and σ as defined in [15]. Therefore, from the log plot of $P_{tr}/\sin(\theta/2)$ versus d, the transfer strength (f_0) and slope parameters (α) can be determined. The transfer probability for the system of $^{16}O + ^{208}Pb$ is calculated using the transfer angular distributions obtained from the CRC code. The coupling scheme is given as in [2]. Figure 4a shows a plot of this transfer probability versus d at 80 MeV for the neutron transfer channel. The neutron transfer to the ground state of ^{209}Pb and to the various excited states are combined into one effective neutron transfer probability. Figure 4b shows the proton and alpha transfer probabilities at 80 MeV. The proton transfer probability to the ground state (squares) and the excited state (plus symbols) of ^{209}Bi are shown separately in figure 4b. As seen in the figure for proton transfer case, the slope parameters for a given particle transfer to various excited states are similar.

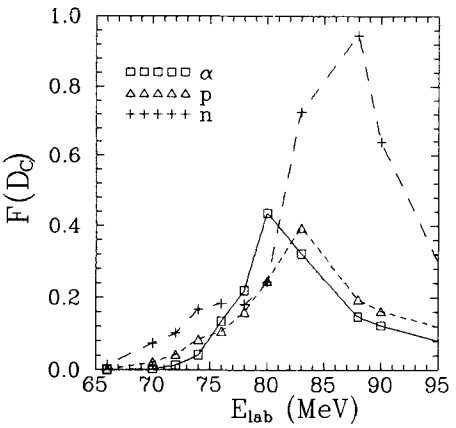

Figure 5. Transfer strength function at closest approach ($F(D_c)$) versus lab energy, for different transfer channels. The symbols represent energies where the calculations were performed and intrapolated by the respective curves.

Therefore, the strength of a given particle transfer to ground state and various excited states are combined into effective one channel transfer strength.

Figure 5 shows the variation of effective one channel transfer strength as a function of incident energy evaluated at the distance of closest approach (D_c). The strong r dependence of eq. (8c) is cancelled at D_c and therefore the effects of channel couplings on transfer strength can be seen at D_c. It is seen from the figure that the effective transfer channel strength evaluated along a Coulomb trajectory, shows rapid variation as a function of energy. The strength attains maximum at around the barrier energies depending on the Q-values of the channels and decreases on either side of the barrier energies, as a result of couplings. However, at high energy the transfer strength parameters will be modified owing to nuclear branch of semiclassical deflection function [16].

Following this method, the effective transfer strength consistent with experimental transfer angular distributions can be determined. This effective transfer strength can then be used in the simplified coupled channel codes like CCFUS in order to estimate approximately the fusion enhancement due to transfer couplings [15]. The experimental data of $^{16}O + ^{208}Pb$ system for nitrogen and carbon channels [12] was analyzed at 80, 88 and 90 MeV and the transfer strength at the barrier position was estimated. Similar calculations were performed for the $^{16}O + ^{232}Th$ system from the available experimental data at various energies [17, 18]. For this system, the transfer strength was combined into two effective one and two proton transfer channels. The parameters thus estimated are listed in table 3. The transfer strength functions at R_b for various cases are seen to be strongly energy dependent. This is expected and as discussed in the previous section, the channel couplings renormalize the transfer strength (refer to figure 5).

The predictions for fusion cross section and mean square spin from the CCFUS code following this method are listed in table 4 for $^{16}O + ^{208}Pb$ system. The other parameters used in CCFUS code are also given. The experimental data are tabulated for comparison. It is seen that the results of the present method for fusion $\langle L^2 \rangle$

Table 3. Transfer function parameters extracted following semi-classical analysis of experimental data [12, 17, 18] and used as input parameters to CCFUS.

(a) $^{16}O + ^{208}Pb$ system; $\Delta V = 22{\cdot}0$, $V_b = 75{\cdot}92$ MeV, $R_b = 11{\cdot}7$ fm, $\hbar\omega = 4{\cdot}78$ MeV, Q_g (nitrogen) = 0·658 MeV and Q_g (carbon) = 4·7 MeV.

E_{lab}(MeV)	$F(R_b)$ (nitrogen)	$F(R_b)$ (carbon)
80	1·26	1·93
88	0·6	0·62
90	0·48	0·37

(b) $^{16}O + ^{232}Th$ system; $\Delta V = 22{\cdot}0$, $V_b = 81{\cdot}70$ MeV, $R_b = 11{\cdot}96$ fm, $\hbar\omega = 4{\cdot}7$ MeV, Q_g (nitrogen) = 2·9 MeV and Q_g (carbon) = 9·0 MeV.

E_{lab} (MeV)	$F(R_b)$ (nitrogen)	$F(R_b)$ (carbon)
80	0·52	0·49
83	0·59	0·52
86	0·64	0·41
92	0·545	0·43
105	0·417	0·46

Table 4. Results for fusion of $^{16}O + ^{208}Pb$ system (For comparison with CRC results using FRESCO refer to table 2).

E_{lab}	σ_f(mb)	$\langle L^2\rangle(\hbar^2)$	$\sigma_{f,exp}$(mb)	$\langle L^2\rangle_{exp}(\hbar^2)$
80	37	191	36 ± 4	200 ± 20
88	312	426	350 ± 40	
90	397	425	377 ± 50	430

are in agreement with experimental data. However the estimates of the present method for fusion $\langle L^2\rangle$ are higher than FRESCO estimates, especially at low energy (see table 2). The corresponding L-distributions for 80 MeV case are shown in figure 6. It is seen that the present method using CCFUS code predicts much broader fusion L-distribution compared to both 1DBPM and FRESCO. This discrepancy between the present method and the FRESCO at 80 MeV is not expected because the CRC transfer form factors were adjusted in FRESCO at 80 MeV in order to match the CRC integrated transfer cross sections with experimental data. However, it was observed that though the integrated cross sections at this energy match, the predicted transfer angular distributions are not in good agreement with the experimental data of [12]. In the present method, we are extracting the transfer strength consistent with experimental data. Therefore this effectively includes all significantly

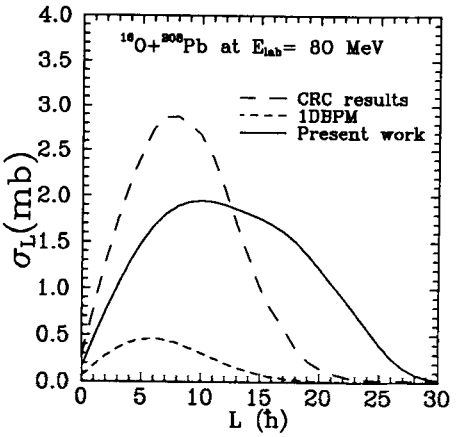

Figure 6. Fusion L-distributions from the present method using CCFUS (solid curve), FRESCO (long dashes) and one dimensional BPM results (short dashed curve).

contributing channels in addition to all higher order coupling effects. Further, this discrepancy may also be due to the reason that the CCFUS calculations treat the coupling form factors in constant coupling approximation, evaluated at the barrier position. In the case of $^{16}O + ^{232}Th$, the transfer couplings do not appreciably effect the fusion results as reported by Esbensen *et al* [19] and the enhancement in fusion excitation function is dominantly due to permanent deformation of the target (^{232}Th).

Summary

The E and L dependence of effective elastic channel potentials implicit through the variable ε is shown to be a good approximation. Further, the dispersion relation in ε variable is shown to be valid at the strong absorption radius. The DR is also studied at other radial separations. The ε dependence for elastic channel potential is shown to be consistent with the experimental data for both elastic and fusion channels. The variation of effective transfer strength as a function of energy is obtained using the transfer angular distributions of the CRC code. It is observed that the variation of effective transfer strength, estimated along a Coulomb trajectory, is similar to the TA seen in the elastic channel case. It is seen that the effective transfer strength derived from experimental transfer angular distributions can account for both the fusion cross section enhancement and its mean square spin.

Acknowledgements

The authors are thankful to Dr I J Thompson for providing the FRESCO code, and Drs S S Kapoor, A K Mohanty, D M Nadkarni, A K Jain, R S Mackintosh and M A Nagarajan for very fruitful discussions during the course of this work. The referee is acknowledged for important suggestions.

References

[1] M A Nagarajan, C C Mahaux and G R Satchler, *Phys. Rev. Lett.* **54**, 1136 (1985)
[2] I J Thompson, M A Nagarajan, J S Lilley and M J Smithson, *Nucl. Phys.* **A505**, 84 (1989)
[3] G R Satchler, *Phys. Rep.* **199**, 147 (1991)
[4] P Singh, S Kailas, A Chatterjee, S S Kerekatte, A Navin, A Nijasure and B John, *Nucl. Phys.* **A555**, 606 (1993)
[5] B T Kim, H C Kim and K E Park, *Phys. Rev.* **C37**, 998 (1988)
[6] A K Mohanty, S V S Sastry, S K Kataria and V S Ramamurthy, *Phys. Rev. Lett.* **65**, 1096 (1990)
[7] A K Mohanty, S V S Sastry, S K Kataria, S Kailas and V S Ramamurthy, *Phys. Lett.* **B247**, 215 (1990)
[8] J A Christley, M A Nagarajan and I J Thompson, *J. Phys.* **G17**, L163 (1991)
[9] S V S Sastry, A K Mohanty and S K Kataria, *Pramana – J. Phys.* **41**, 525 (1993)
[10] S G Cooper and R S Mackintosh, *Nucl. Phys.* **A513**, 373 (1990)
[11] V L M Franzin and M S Hussein, *Phys. Rev.* **C38**, 2167 (1988)
[12] F Videbaek, R B Goldstein, L Grodzins, S G Steadman, T A Belote and J D Garrette, *Phys. Rev.* **C15**, 954 (1977)
[13] E Vulgaris, L Grodzins, S G Steadman and R Ledoux, *Phys. Rev.* **C33**, 2017 (1986)
[14] J B Ball, C B Fulmer, E E Gross, M L Halbert, D C Hansley, C A Ludemann, M J Saltmarsh and G R Satchler, *Nucl. Phys.* **A252**, 208 (1975)
[15] L Corradi, S J Skorka, U Lenz, K E G Lobner, P R Pascholati *et al*, *Z. Phys.* **A335**, 55 (1990)
[16] C V K Baba, V M Datar, K E G Lobner, A Navin and F J Schindler, *Phys. Lett.* **B338**, 147 (1994)
[17] J S Karp, S G Steadman, S B Gazes, R Ledoux and F Videbaek, *Phys. Rev.* **C25**, 1838 (1982)
[18] J P Lestone, J R Leigh, J O Newton and J X Wei, *Nucl. Phys.* **A509**, 178 (1990)
[19] H Esbensen and S Landonwe, *Nucl. Phys.* **A467**, 136 (1987)